CHEMISTRY OF MATERIALS

Open Access

pubs.acs.org/cm

Article

Sustainable Synthesis and Benchmark CO_2 Uptake in a Zn-Triazole-Based MOF and Its Processable PVDF Composite

Armando Rigamonti,[§] Charl X. Bezuidenhout,[§] Jacopo Perego, Erica Montanari, Angiolina Comotti,* and Silvia Bracco*

Cite This: *Chem. Mater.* 2026, 38, 4038−4045

Read Online

ACCESS | Metrics & More | Article Recommendations | Supporting Information

ABSTRACT: Pillared-layer metal−organic frameworks (MOFs) comprising triazolate and oxalate or organodicarboxylate linkers are emerging materials for selective CO_2 capture in large-scale applications. One key aspect to consider for industrial applications is the search for synthetic strategies that minimize the use of solvents, thereby reducing the environmental impact and improving scalability. Herein, a protocol that combines liquid-assisted mechanochemistry and incubation with a minimal amount of solvent was applied to produce both a triazolate-fumarate Zn-MOF and a MOF-polymer composite shaped into self-supporting cylindrical objects amenable to CO_2 capture even under humid conditions. The Zn-MOF exhibits the highest surface area and CO_2 adsorption capacity in this class of materials, and a CO_2/N_2 selectivity of 200 at 273 K. A 36 kJ/mol value of heat of adsorption was estimated by direct measurement of the heat exchanged upon stepwise CO_2 loading, in tandem with a CO_2 adsorption isotherm. Upon one hundred CO_2 adsorption/desorption cycles, the Zn-MOF exhibits remarkable cycling stability. Breakthrough experiments with CO_2/N_2 mixtures containing 5, 10, and 15% CO_2 unveiled selective CO_2 adsorption even in the presence of humidity (up to 15%) and full recovery of the composite sorption performance through solvent incubation. In-depth spectroscopic and diffractometric characterization of the activated material and its composite revealed the sophisticated and dynamic arrangement of pillars and layers within the framework. *In situ* powder X-ray diffraction (PXRD) during CO_2 loading and unloading, combined with *ab initio* computational studies, enabled the determination of the preferred CO_2 adsorption sites within the framework.

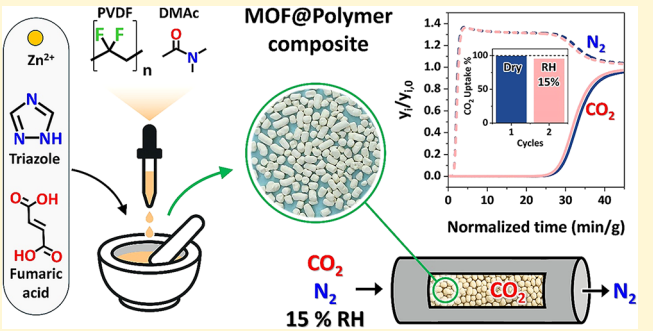

INTRODUCTION

Global warming affects a significant portion of the planet, including both temperate regions and countries already experiencing ongoing desertification.[1] In this context, the emission of carbon dioxide, primarily from fossil fuel combustion processes, is considered to be a key factor. Among CO_2 capture technologies, scrubbing processes with aqueous amine solutions are currently employed, although they present a few drawbacks, such as energy-demanding regeneration and waste management.[2,3]

One of the promising alternatives being explored involves the use of solid absorbents capable of selectively capturing CO_2 from industrial combustion fumes. In the literature, several classes of materials have been proposed, including metal−organic frameworks (MOFs), covalent-organic frameworks (COFs), porous-organic frameworks (POPs), and hydrogen-bonded organic frameworks.[4−14] In this context, metal−organic frameworks (MOFs) offer significant advantages for storing gases and capturing CO_2 selectively with respect to other gases, owing to their large surface area, tunable pore size, and chemical versatility.[15−21]

Recently, the effectiveness of CALF-20, a MOF discovered by G. Shimizu's group at the University of Calgary, in capturing CO_2 in the presence of air humidity has been demonstrated, and its deployment at an industrial scale is currently underway.[22−24] In addition, to fulfill the requirements of stability, scalability, and easy regenerability, the competition of CO_2 vs water adsorption sites resulted in its fruitful and successful application. This MOF belongs to the class of pillared-layer MOFs[25−27] and specifically consists of two-dimensional zinc-coordinated 1,2,4-triazolate layers and oxalate pillars. Several triazolate-based Zn-MOFs have been studied, containing either functionalized triazolate molecules modified with amino and methyl groups or substituting the oxalate linker with organodicarboxylate pillars, such as

Received: November 30, 2025
Revised: April 2, 2026
Accepted: April 7, 2026
Published: April 11, 2026

https://doi.org/10.1021/acs.chemmater.5c03237
Chem. Mater. 2026, 38, 4038−4045

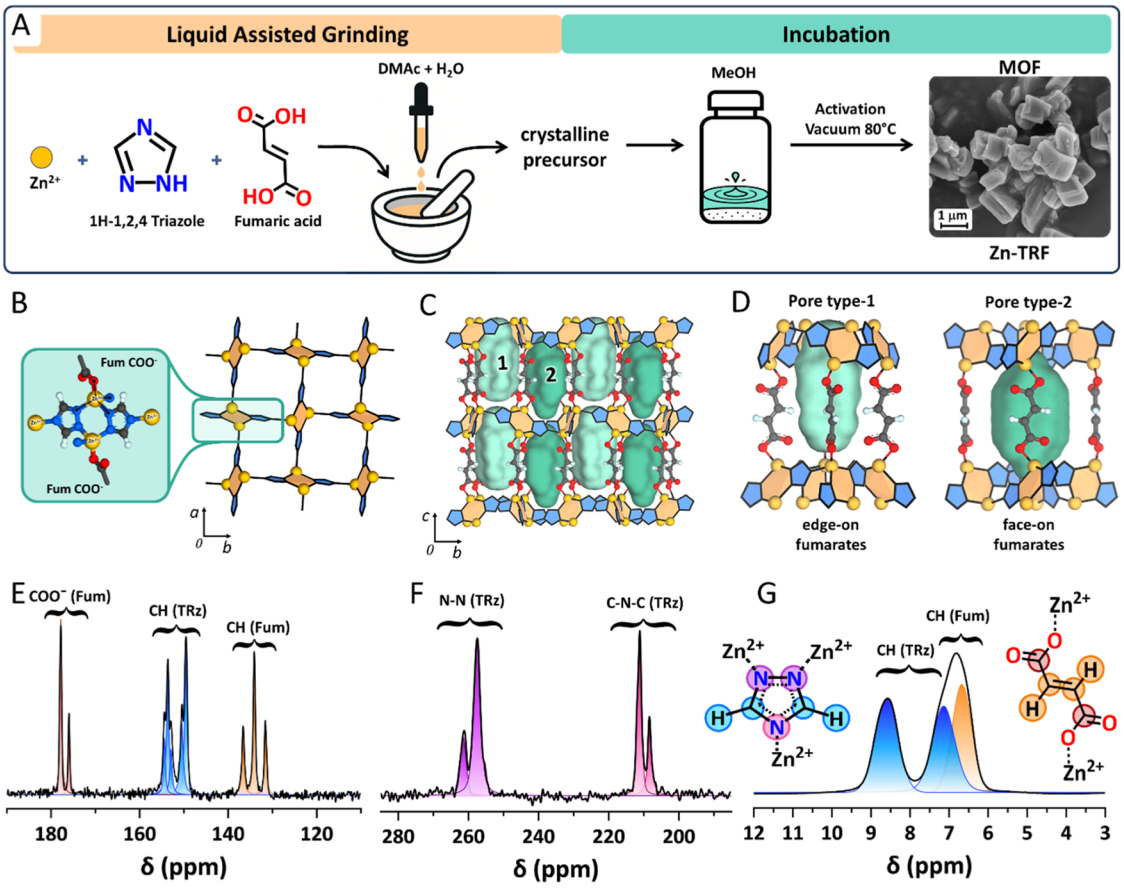

Figure 1. Zn-TRF: preparation and structural analysis. (A) Zn-TRF preparation: scheme of liquid-assisted mechanochemistry synthesis followed by MeOH incubation. Right − SEM images of micron-sized crystals of Zn-TRF. (B) Crystal structure of activated Zn-TRF obtained from the Rietveld refinement of *in situ* PXRD collected under vacuum at 298 K using a synchrotron light source. Left − binuclear metal node highlighting the tetrahedral coordination geometry of the zinc cations and the connectivity of 1,2,4-triazolate ligands. Right − the Zn-triazolate 2D layer as viewed along the *c*-axis direction. (C) Crystal structure viewed along the *a*-axis, showing the pillaring of the 2D layers by fumarate ligands and the two unique pores generated. (D) Differentiation between pore-1 and pore-2, based on the orientation of the fumarate ligands with respect to the pore. For parts (C, D), the pores were partitioned using dummy atoms for visual clarity and mapped using a probe of 1.3 Å. (E) 150.8 MHz ^{13}C CP MAS NMR spectrum, (F) 49.5 MHz ^{15}N CP MAS NMR spectrum, and (G) 600 MHz ^{1}H MAS NMR spectrum with a spinning speed of 30 kHz.

fumarate and terephthalate linkers, showing promising performances in gas adsorption and separation.[28−32]

Here, a pillared-layer triazolate-based Zn-MOF, with benchmark CO_2 uptake capacity in this class of materials under operating conditions of 298 K and 1 bar (4.8 mmol/g, 21.1 wt %), was obtained by a combined liquid-assisted grinding and solvent incubation (LAG-IN) method. The method represents a sustainable alternative to conventional synthesis techniques, owing to its limited solvent consumption.[33−36] The Zn-MOF, composed of triazolate (TRz) and fumarate (Fum) ligands (denoted Zn-TRF), achieves a CO_2/N_2 (15/85) selectivity as high as 200 at 273 K at low coverage and complete cyclability over 100 cycles. Cylindrical pellets of MOF-polymer composites were formed *in situ* by cogrinding MOF precursors in the presence of hydrophobic poly(vinylidene difluoride) (PVDF), followed by extrusion and incubation. Dynamic breakthrough experiments demonstrated the selective CO_2 uptake with respect to N_2 in the presence of humidity and its complete recovery by exposure to MeOH vapors at room temperature, proving the composite performances for large-scale CO_2 uptake applications. A synergistic approach was employed to monitor both activated and *in situ* CO_2-loaded materials, based on Fourier transform infrared (FT-IR) and ^{1}H−^{13}C MAS NMR spectroscopies, scanning electron microscopy (SEM), microcalorimetry simultaneously detected with CO_2 adsorption isotherm, and synchrotron-source powder X-ray diffraction (PXRD) coupled with density functional theory (DFT) calculations, in order to unravel the framework structure and the most favorable CO_2 binding sites for optimal performances.

RESULTS AND DISCUSSION

The Zn-TRF was synthesized via a liquid-assisted mechanochemical approach, followed by methanol incubation (Figure 1). Basic zinc carbonate $[ZnCO_3]_2[Zn(OH)_2]_3$ was ground with fumaric acid (H_2Fum) and 1H-1,2,4-triazole (HTRz) in the presence of a small amount of dimethylacetamide (DMAc) and water (Figure 1A), yielding a crystalline precursor, which, upon subsequent incubation in methanol at 120 °C for 17 h, produces the final MOF material, Zn-TRF·*x*MeOH (Figure S1). The resulting material was activated under a high vacuum at 80 °C to remove residual solvent molecules, producing a highly porous framework. This two-step method involving a minimal amount of solvent proved to be particularly effective for the synthesis of Zn-TRF with a high yield (78%).

The FT-IR spectrum of the activated MOF displayed a band at 1660 cm^{-1}, attributed to the asymmetric stretching vibration

https://doi.org/10.1021/acs.chemmater.5c03237
Chem. Mater. 2026, 38, 4038−4045

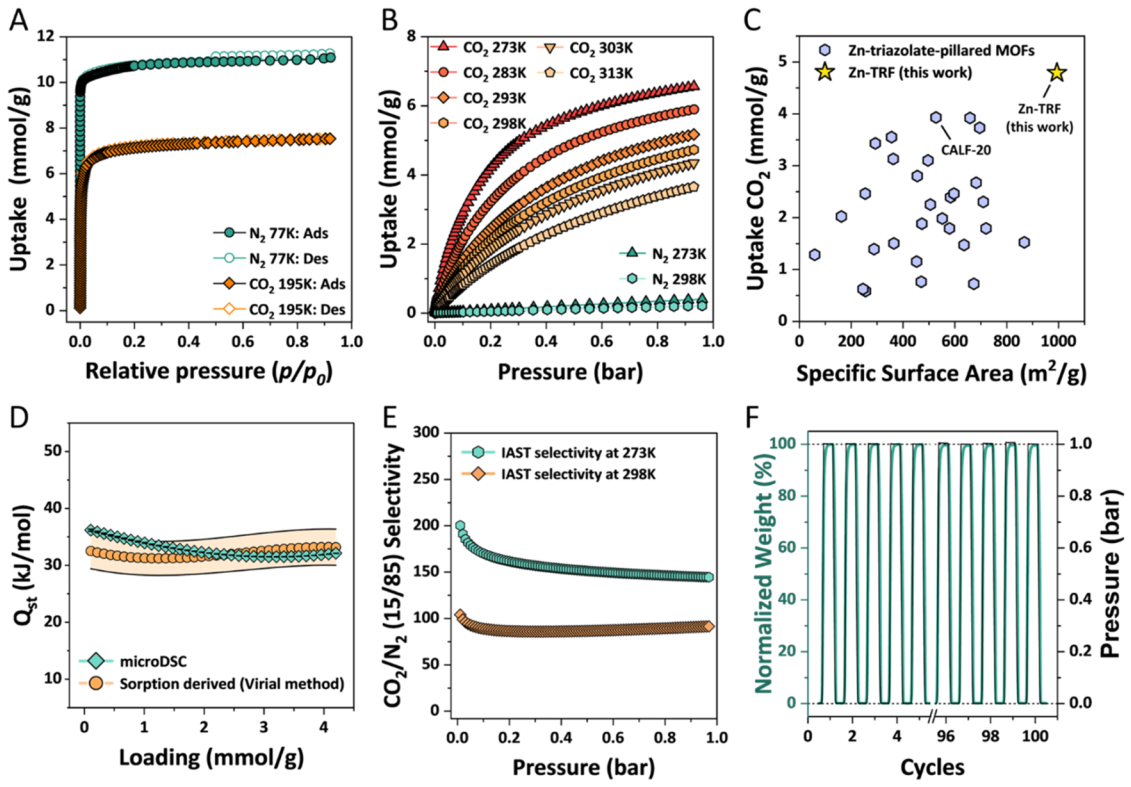

Figure 2. Activated Zn-TRF: (A) N_2 and CO_2 adsorption isotherms at 77 and 195 K, respectively. (B) CO_2 and N_2 adsorption isotherms from 273 to 313 K and from 273 to 298 K, respectively. (C) CO_2 uptake at 1 bar and 298 K versus surface area. Zn-TRF as compared to pillared-layer Zn-triazolate MOFs. (D) Isosteric heat of adsorption (Q_{st}) of CO_2 at 293 K measured via microcalorimetry (green diamonds), and comparison with the values calculated from CO_2 adsorption isotherms using the virial method (orange circles). (E) CO_2/N_2 selectivity calculated using IAST theory for a 15/85 CO_2/N_2 mixture at 273 and 298 K. (F) CO_2 adsorption and desorption cyclability at 1 bar by gravimetric measurements.

of the carboxylate group, with a shift of 73 cm^{-1} from the free C═O value of fumaric acid, indicative of coordination to Zn^{2+} ions (Figure S2). ^1H NMR of digested Zn-TRF enabled quantification of the ligand content (Figure S3), which corresponds to 1.8:1 for triazolate and fumarate ligands, respectively, in agreement with the 2:1 stoichiometric ratio of the crystallographic model (see later). The triazolate content was slightly underestimated due to the exchange of CH hydrogen under acidic conditions. The thermal stability of Zn-TRF was evaluated by thermogravimetric analysis in air, revealing high stability up to temperatures of >250 °C (Figure S4). The residue, corresponding to 41.8 wt %, agrees with the stoichiometry determined by the solution ^1H NMR spectrum.

The activated structure was resolved by a combination of Rietveld refinement and PW-DFT optimization of the PXRD pattern collected using a synchrotron radiation source, revealing the presence of two phases: a major (84.3%) and a minor phase (15.7%), which crystallized in the *P*-4*c*2 and *P*4/*n* space groups, respectively (Figures 1B, S6, and Table S2). In both phases, the Zn^{2+} ions are coordinated to three TRz nitrogen atoms and one oxygen atom of the fumarate ligand, adopting a distorted tetrahedral coordination geometry. The triazolate ligands bridge pairs of Zn^{2+} ions to form binuclear nodes that further connect to one another, extending in the *ab*-plane to form 2D layers. The fumarate ligands form a monodentate coordination to the Zn^{2+} ions, pillaring the 2D layers and generating an extended 3D network with a *pcu* topology.[37] For the main phase, the double bond oxygen atom of the Fum carboxylates forms C═O···H−C interactions with the C−H groups of two triazolate ligands with an O···H distance of 2.6 Å each. The major and minor phases exhibit different spatial relationships between neighboring 2D layers, adopting A-A-A-A and A-B-A-B configurations (Figure S7), respectively, resulting in distinct pore topologies for the two phases. The major phase possesses two types of pores, pore-1 and pore-2, with cross-sectional dimensions of 4.1 × 4.1 and 3.8 × 7.8 $Å^2$, respectively (Figure 1C,1D). Instead, the minor phase exhibits three types of interconnected pores with cross-sectional dimensions of 5.5 × 5.5 $Å^2$, 3.9 × 3.9 $Å^2$, and 2.4 × 7.9 $Å^2$, respectively. The two types of pores in the main phase are enclosed by fumarate linkers and interconnected through the spaces between the fumarate ligands. The two pores can be differentiated by the orientation of the fumarate with respect to the pore wall: pore-1 has the Fum linkers oriented edge-on with respect to the pore wall, with the C−H groups directed into the pore , while pore-2 has the Fum linkers oriented face-on with respect to the pore wall. Both pores are decorated face-on by the triazole rings (along the *c*-axis) and the triazole C−H groups at the top and bottom.

^{13}C CP MAS NMR spectrum shows two families of signals, each containing signals corresponding to COO^- (Fum), CH(TRz), and CH(Fum) carbons. The two families of signals differ in intensity, with one set being dominant and the other being weaker, corresponding to the major and minor phases, respectively (Figure 1E). The quantitative evaluation, performed from fully relaxed ^{13}C MAS NMR (Figure S10), corresponds to a 4:1 ratio between the two phases, in agreement with the PXRD data. Similarly, the ^{15}N CP MAS NMR spectrum exhibits two dominant signals separated by 50.3 ppm associated with the two distinct nitrogen species in

https://doi.org/10.1021/acs.chemmater.5c03237
Chem. Mater. 2026, 38, 4038−4045

the major phase, while the lower intensity peaks are due to the presence of the minor phase (Figures 1F, S13, and Table S4). Regarding the multiplicity of signals, the two phases are also recognized by the different symmetry of unit cells: the fumarate COO^- and CH_{Fum} carbons are equivalent by symmetry in the major phase each of them generating one single signal, whereas two signals for each species are detected for the minor phase, in agreement with the lower symmetry of crystal structure (Figures 1E and S11). The ^1H MAS NMR spectrum provides relevant information about the presence of intermolecular interactions between CH_{TRz} and one of the oxygens of the carboxylate (Figure 1G). Two resonances with a large 1.5 ppm separation are detected, which is consistent with the two distinct $C-H_{TRz}\cdots O$ interactions ($H_{TRz}\cdots O$ distances of 2.6 and 3.0 Å), as observed in the crystal structure (Figure S11). The two distinct environments are confirmed by the ^{13}C CP MAS spectrum, showing two main ^{13}C resonances for CH_{TRz} separated by 3.8 ppm. The overall resonance assignments for ^1H, ^{13}C, and ^{15}N nuclei were supported by chemical shift predictions of the minimized crystal structures, utilizing the PW-DFT-based CASTEP code and the GIPAW method for the calculation of the NMR shielding constants. (Figures S9−S13).

The porosity of Zn-TRF was confirmed by N_2 adsorption isotherms measured at 77 K, yielding Langmuir and Brunauer−Emmett−Teller (BET) surface areas of 995 and 978 m^2/g, respectively (Figure 2A). These are the highest values reported so far for the family of Zn-triazole-dicarboxylate pillared MOFs (Table S5),[27−30] demonstrating that the combined synthetic approach of mechanochemistry followed by MeOH incubation is an effective method to enhance the crystallinity of the material. An independently synthesized batch exhibited comparable adsorption performance compared to that of the original sample (BET surface area 1004 m^2/g; N_2 uptake 11.3 mmol/g at 77 K), confirming the robustness of the preparation procedure (Figures S14, S15, and Table S6). To evaluate the capacity of Zn-TRF to selectively capture CO_2 with respect to N_2, adsorption isotherms of both gases were carried out at various temperatures from 273 to 313 K. Zn-TRF adsorbs 4.79 mmol/g (21.1 wt %) at 298 K, while a negligible N_2 amount is detected (Figure 2B). Notably, the CO_2 uptake at 298 K and 1 bar exceeds the CO_2 uptake values of triazolate-based MOFs under the same conditions (Figure 2C and Table S5). The isosteric heat of CO_2 adsorption (Q_{st}) as a function of loading was determined both from isotherms collected at different temperatures using the virial method and by a direct measurement using a hyphenated approach that combines volumetric adsorption analysis and microcalorimetry (Figures 2D and S16−S19). This setup enabled simultaneous monitoring of gas uptake and heat evolution at 293 K. Calorimetric data at low coverage revealed an isosteric heat of 36 kJ/mol, providing a precise and complementary assessment of the isotherm-derived estimation. This value is comparable to that of the zinc aminotriazolate-acetate-hydroxide pillared MOF, a member of the same family bearing amino-groups (Figure S20 and Table S8). Notably, this value falls within the ideal range for efficient CO_2 capture and separation from N_2 and the low energy demand for CO_2 release.

Selectivity for a 15/85 CO_2/N_2 mixture was evaluated using Ideal Adsorbed Solution Theory (IAST). At 273 K, the material exhibited selectivities of 200 at low coverage (1 mbar) and 144 at 1 bar (Figure 2E). At room temperature, the selectivity is as high as 104 at low coverage and 91 at 1 bar. These values exceed those reported for the same family of materials under similar conditions (Table S8).[38] They are also comparable to those of benchmark MOFs such as UiO-66-$(OH)_2$, UiO-66(Hf)-$(OH)_2$, UTSA-49, and ZnF(daTZ).[39,40] IAST analysis further reveals that for a gas mixture containing 15% CO_2 and 85% N_2 at a total pressure of 1 bar, the material exhibits a pronounced preference for CO_2 adsorption, resulting in an enrichment of CO_2 in the adsorbed phase up to 94% (Figure S21).

Additionally, one hundred CO_2 adsorption/desorption cycles were performed at a constant temperature of 298 K using a gravimetric analyzer, which continuously recorded the sample's weight variation throughout the process (Figure 2F). Each cycle involved CO_2 adsorption up to 1 bar, with a loading rate of 400 mbar/min, reaching the maximum uptake of 5.2 mmol/g within 15 min. Desorption was achieved by decreasing the CO_2 pressure at the same rate (400 mbar/min), with complete release occurring within 10 min (Figures S24 and S25). Remarkably, after 100 consecutive cycles, the material exhibited only a 0.5% reduction in the maximum CO_2 uptake capacity, underscoring the excellent cycling stability and robust performance of the Zn-TRF MOF under repeated operating conditions.

In situ powder X-ray diffraction of Zn-TRF under CO_2 atmosphere at 1 bar and 298 K shows a change in the diffraction pattern, suggesting a CO_2-induced structural rearrangement which remains stable up to 19 h (Figure S27). Successive activation under a vacuum at 298 K demonstrates a complete recovery of the activated structure (Figure S28). The CO_2-loaded crystal structure, Zn-TRF·CO_2 ($Zn_2TRz_2Fum{\cdot}2CO_2$), was resolved by PW-DFT optimization and Rietveld refinement of PXRD patterns collected under 1 bar of CO_2 at 298 K (Figure S29 and Table S11). The PW-DFT optimizations (in the *Pc* space group) allow the structure to adjust in the presence of the CO_2 molecules, followed by rigid-body Rietveld refinement in the higher symmetry space groups of *P*-4*c*2 (87%) and *P*4/*n* (13%) for the major and minor phases, respectively. The unit cell volume of Zn-TRF·CO_2 increases by 282 $Å^3$ compared with the activated structure. The *c*-axis reduces by 0.56 Å (2.4%) while the *a*- and *b*-axes expand by 0.62 Å (4.8%). The lengthening of the *a*- and *b*-axes can be attributed to the stretching of the zigzag 2D Zn-TRz layers within the *ab*-plane, which also induces a shrinkage perpendicular to the stretching direction, *i.e.*, the *c*-axis. The calculated pore volume (probe radius of 1.82 Å, N_2 kinetic diameter) increases from 0.315 cm^3/g for the activated structure to 0.385 cm^3/g for Zn-TRF·CO_2, which is consistent with the 0.372 cm^3/g pore volume determined from the N_2 adsorption isotherm at 77 K using the α_s-plot analysis method (Figure S26 and Table S9), as recommended by IUPAC.[41]

For the major phase, the Fourier density difference map obtained from the Rietveld refinement showed diffused electron density within the pores, indicating that the CO_2 molecules are highly disordered in both pore-1 and −2 (Figure 3). From the PW-DFT calculations, three main CO_2 binding sites and four unique CO_2 orientations were determined. Two of the binding sites are located in pore-1, which are occupied by CO_2-1 (site-1) and CO_2-2 (site-2) while pore-2 has 4 symmetry equivalent sites (site-3) occupied by two unique CO_2 orientations, CO_2-3 and CO_2-4 (Figure S31).

To compare the binding energy of the main CO_2 site with the Q_{st} at low loading, the binding energy of CO_2-1 in site-1 was calculated by using the activated structure (optimized in

https://doi.org/10.1021/acs.chemmater.5c03237
Chem. Mater. 2026, 38, 4038−4045

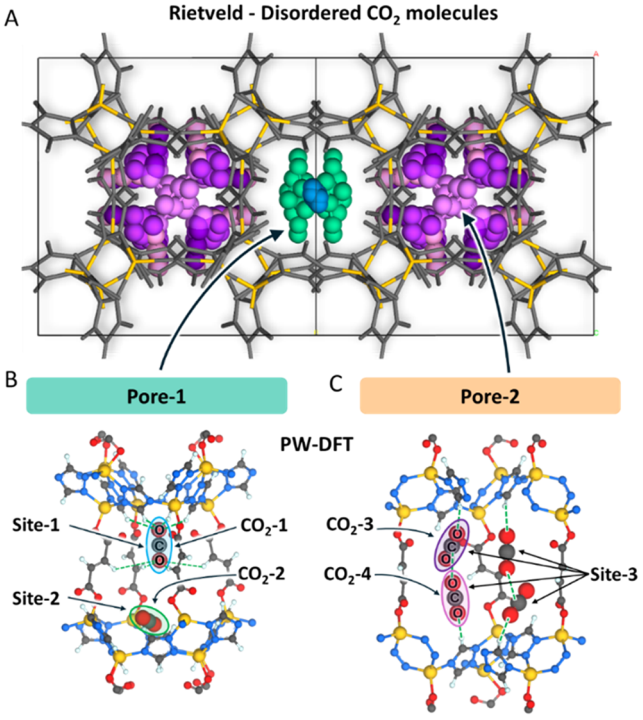

Figure 3. (A) Crystal structure of CO_2-loaded Zn-TRF (viewed along the *c*-axis) obtained from the Rietveld refinement of *in situ* PXRD collected under 1 bar CO_2 gas pressure at 298 K. The CO_2 molecules are highly disordered and shown in space-filling representation, while the MOF framework is shown in stick. The green and blue CO_2 molecules occupy pore-1, while the purple molecules are in pore-2. (B) Two binding sites in pore-1 occupied by CO_2 molecules, CO_2-1 (blue) and CO_2-2 (green). (C) CO_2 molecules, CO_2-3 (purple) and CO_2-4 (light purple) located in the 4 symmetry equivalent binding sites (site-3) within pore-2. The main interactions formed by the CO_2 molecules are shown with green dashed lines.

the presence of CO_2-1), yielding a value of 35 kJ/mol, which is consistent with the Q_{st} of 36 kJ/mol measured by calorimetry. To calculate the binding energies for the other sites, we considered the CO_2-loaded crystal structure. The interaction energies of 30, 33, and 34 kJ/mol for CO_2-2, CO_2-3, and CO_2-4, respectively (average of 32.3 kJ/mol), are in perfect agreement with the experimental value of 32 kJ/mol at high loadings. Moreover, owing to the stretching of the 2D Zn-TRz layers, the tilting of the triazolate groups from 17.4° to 33.3° (with respect to the *ac*- and *bc*-planes) toward the oxygen atoms of CO_2-1 forms multiple C−H···O interactions with D···A of 3.3 − 3.7 Å.

A composite material consisting of Zn-TRF and poly(vinylidene fluoride) (PVDF), denoted Zn-TRF@PVDF, was prepared *in situ* by grinding the MOF reagents with a polymer solution in DMAc, followed by extrusion and incubation, resulting in cylindrical pellets of 1 mm^3 volume (Figure 4A). The incorporation of the fluoropolymer was demonstrated by the presence of its typical FT-IR bands at 840, 877, 1065, and 1276 cm^{-1} (Figure S32) and the ^{13}C resonances at δ = 44.1 and 119.8 ppm for CH_2 and CF_2, respectively, as detected in the ^{13}C MAS NMR spectrum (Figure 4B and Table S12). The amount of polymer in the composite was assessed by ^{13}C MAS NMR to be 14%, in agreement with the quantitative TGA analysis (17 wt %) (Figure S33). CO_2 adsorption isotherms of the composite at room temperature revealed an uptake of 4.54 mmol/g based on the total sample mass, a slight decrease (−5%) compared to the pristine Zn-TRF powder (Figure S37). Considering the amount of polymer in the composite, a more pronounced decrease in the CO_2 capacity would be expected. Indeed, the adsorption capacity, normalized to the Zn-TRF content, showed an increase of approximately 10−14% in the rate of CO_2 uptake compared to the pure MOF powder, suggesting that the synergistic interactions between the MOF and the polymer matrix enhance the adsorption performance of the framework.

Dynamic breakthrough adsorption experiments were carried out to evaluate the performance of the Zn-TRF@PVDF composite in the separation of CO_2/N_2 gas mixtures (Figure 4C). CO_2/N_2 binary gas mixtures containing 5%, 10%, and 15% CO_2 were tested with a total flow rate of 6 sccm. At 298 K and 1 bar, the amount of CO_2 adsorbed by the composite was found to be 0.58 mmol/g, 1.00 mmol/g, and 1.37 mmol/g, respectively, in good agreement with the values predicted by IAST calculations (Figure S38). Furthermore, using a CO_2/N_2 mixture with a 15/85 ratio, the material exhibited excellent stability over multiple adsorption/desorption cycles, with no observable loss in performance (Figure 4D).

To explore the performance of the composite under operating conditions in the presence of humidity, breakthrough experiments were conducted by using a CO_2/N_2 mixture with 5% relative humidity (Figure S40). Notably, no reduction of the level of CO_2 uptake was observed as compared to the first run carried out under dry conditions. In the case of 15% humidity, a 6% decrease of CO_2 uptake was detected (Figure S40); however, after exposure to methanol vapor (N_2 carrier) for 8 h at 25 °C and solvent removal at 80 °C for 30 min (under He flow), the pellets' adsorption capacity was fully restored, as detected by the breakthrough analysis under dry conditions. The X-ray diffraction pattern of the composite confirms the crystal structure of the Zn-TRF@PVDF (Figures S41−S43). Thus, the solvent-exchange regeneration strategy provides a practical tool that ensures reproducible cyclic performance and displaces adsorbed water, restoring the pore capacity. Furthermore, the impact of H_2O on CO_2 adsorption was investigated by comparing the H_2O breakthrough curves at 15% RH using CO_2 and N_2 as carrier gases, respectively, for Zn-TRF@PVDF (Figure 4E). The water uptake (4.4 mmol/g) using N_2 as a carrier gas is in excellent agreement with the water adsorption isotherm at 0.15 p/p_0 and 298 K (Figure S44). The two breakthrough curves follow markedly different profiles with a shorter breakthrough time of the water front observed in the presence of CO_2, demonstrating effective competition of CO_2 with H_2O for the adsorption sites (Figure 4E). A similar behavior was observed in the case of CALF-20, wherein the CO_2/H_2O competition is virtually complete.[42]

CONCLUSIONS

The synthetic protocol, which comprises liquid-assisted grinding and incubation, enabled the formation of a highly crystalline triazolate-organodicarboxylate MOF with the highest surface area and the highest CO_2 adsorption capacity within this family of materials. Additionally, this synthesis method was proven to be effective for the *in situ* formation of the MOF in the presence of a polymer, producing a composite with a controlled morphology. Indeed, the composite paste can be extruded into self-standing objects of predefined size and shape, while preserving gas adsorption performance. Breakthrough experiments demonstrated the selective uptake of CO_2

https://doi.org/10.1021/acs.chemmater.5c03237
Chem. Mater. 2026, 38, 4038−4045

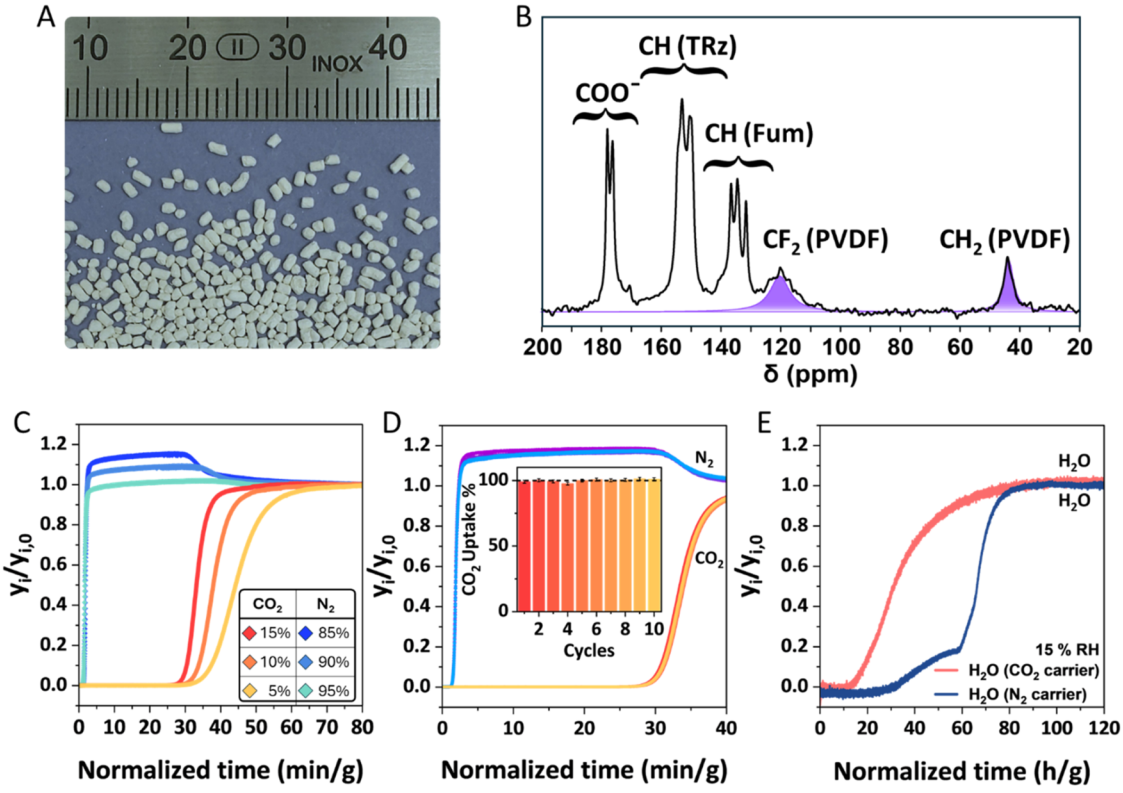

Figure 4. (A) Zn-TRF@PVDF cylindrical pellets with an average size of approximately 1 × 1 × 1 mm^3 after ten consecutive breakthrough measurements. (B) Quantitative ^{13}C SPE MAS spectrum collected with a recycle delay of 60 s of activated Zn-TRF@PVDF composite. (C) Breakthrough curves for CO_2/N_2 separation at varying gas compositions (CO_2 partial pressures of 0.05, 0.1, and 0.15), recorded at 298 K and ambient pressure with a total flow rate of 6 sccm. (D) Ten consecutive breakthrough cycles for CO_2/N_2 separation (15/85 mixture) carried out at 298 K. Regeneration was performed after each cycle using a He flow (6 sccm) at 298 K. The inset shows normalized CO_2 uptake with respect to the first cycle, demonstrating stability over repeated use. (E) Breakthrough profiles of H_2O measured at 15% relative humidity under single-component and competitive conditions at 298 K. The single-component H_2O experiment conducted using N_2 as the carrier gas (blue line) is compared with the competitive H_2O experiment performed using CO_2 as the carrier gas (orange line).

over N_2 even in the presence of humidity and complete regeneration by solvent incubation. *In situ* PXRD upon CO_2 loading, combined with DFT calculations, revealed primary sorption sites endowed with multiple C−H···O interactions between CO_2 and the triazolates.

In summary, the moderate solvent consumption enables the realization of a sustainable chemistry process for the synthesis of solid CO_2-adsorbing materials. Furthermore, this versatile method opens up stimulating perspectives for the preparation of both MOFs and their composites on an industrial scale.

EXPERIMENTAL SECTION

Materials

All chemicals were used as received from commercial suppliers without further purification.

Synthesis

Preparation of Zn-TRF. A total of 109.8 mg (1 mmol of Zn^{2+}) of the salt $[ZnCO_3]_2[Zn(OH)_2]_3$, 69 mg (1 mmol) of 1H-1,2,4-triazole, and 58 mg (0.5 mmol) of fumaric acid are weighed and placed in an agate mortar. A first dry grinding is performed for approximately 5 min. Subsequently, 0.2 mL of anhydrous dimethylacetamide and 0.05 mL of water are added, and grinding is continued until the powder is completely dry. A second liquid-assisted grinding (LAG) is then carried out using the same amounts of dimethylacetamide (0.2 mL) and water (0.05 mL) as in the first LAG step. The resulting powder is transferred to an 8 mL vial, and 1 mL of methanol (MeOH) is added. The vial is sealed and placed in an oven at 120 °C for 17 h. After thermal treatment, the sample is allowed to cool slowly to room temperature. It is then centrifuged, the supernatant is removed, and the solid is washed three times with 7 mL of MeOH (after activation, 148.6 mg, yield 78.0%).

Preparation of the Zn-TRF@PVDF. A total of 439.2 mg (4 mmol) of $[ZnCO_3]_2[Zn(OH)_2]_3$, 276 mg (4 mmol) of 1*H*-1,2,4-triazole, and 232 mg (2 mmol) of fumaric acid are weighed and placed in an agate mortar. After an initial dry grinding for approximately 5 min, 1.27 mL of a solution of poly(vinylidene fluoride) (PVDF) in dimethylacetamide (DMAc) at a concentration of 150 mg/mL is added. The mixture is ground until a plasticine-like consistency is obtained. The resulting paste is extruded into a methanol bath. The rod-shaped pellets are then collected, transferred to a 40 mL vial, and incubated with 4 mL of MeOH in an oven at 120 °C for 17 h. After incubation, the sample is cooled to room temperature. The supernatant is removed, and the pellets are washed three times with 10 mL of MeOH (after activation, 723 mg, yield 78.8%).

METHODS

Solution NMR spectra were recorded on a Bruker Avance Neo spectrometer (400 MHz, 9.4 T) at 25 °C. TGA was performed on a Mettler Toledo Star System 1 instrument (30−1000 °C, 10 °C/min, air). FT-IR spectra were collected on a Thermo Scientific Nicolet iS20 equipped with an ATR module (550−4000 cm^{-1}). SEM images were acquired on a Zeiss Gemini 500. PXRD patterns were collected on a Rigaku SmartLab (Cu−Kα, 40 kV, 30 mA), including in situ activation (up to 353 K) and measurements under dynamic vacuum and 1.1 bar of CO_2 at 298 K. Synchrotron PXRD data were collected at ESRF (ID22, λ = 0.35431683 Å) using capillary-based measurements under dynamic vacuum. Rietveld refinements were performed

https://doi.org/10.1021/acs.chemmater.5c03237
Chem. Mater. 2026, 38, 4038−4045

using TOPAS-Academic64 V6 software. Periodic DFT calculations were carried out using the CASTEP code (GGA-PBE-D). Solid-state NMR experiments (^{13}C, ^{1}H, and ^{15}N) were performed under MAS on Bruker spectrometers (7.04 and 14.1 T).

Samples were activated at 80 °C under high vacuum ($p < 3 \times 10^{-6}$ bar) prior to sorption measurements. N_2 adsorption isotherms at 77 and 298 K and CO_2 isotherms (195−313 K) were measured on a Micromeritics 3Flex instrument, whereas H_2O adsorption isotherms were collected on a Micromeritics ASAP 2020 system equipped with a vapor accessory. Surface area and porosity were evaluated by BET, Langmuir, α-s plot, t-plot, and NLDFT methods using MicroActive 7.00 software. CO_2 adsorption microcalorimetry was performed by using a Micromeritics ASAP 2050 instrument coupled to a Setaram microDSC7 Evo. IAST selectivity was calculated using RUPTURA software. Breakthrough experiments were performed on a Micromeritics SAA system coupled to a Pfeiffer ThermoStar mass spectrometer with high-purity gases (N_2 5.0, He 5.0, and CO_2 4.5). Measurements were carried out at 25 °C with CO_2/N_2 mixtures (5−15%) at a total flow rate of 6 sccm.

■ ASSOCIATED CONTENT

Supporting Information

The Supporting Information is available free of charge at https://pubs.acs.org/doi/10.1021/acs.chemmater.5c03237.

Synthetic procedures, experimental methods, supporting figures, and tables for structural characterization of Zn-TRF and Zn-TRF@PVDF composite (PDF)

Accession Codes

Deposition Numbers 2495999−2496002 contain the supplementary crystallographic data for this paper. These data can be obtained free of charge via the joint Cambridge Crystallographic Data Centre (CCDC) and Fachinformationszentrum Karlsruhe Access Structures service.

■ AUTHOR INFORMATION

Corresponding Authors

Angiolina Comotti − *Department of Materials Science INSTM Research Unit, University of Milano-Bicocca, 20125 Milan, Italy*; orcid.org/0000-0002-8396-8951; Email: angiolina.comotti@unimib.it

Silvia Bracco − *Department of Materials Science INSTM Research Unit, University of Milano-Bicocca, 20125 Milan, Italy*; orcid.org/0000-0002-2575-6424; Email: silvia.bracco@unimib.it

Authors

Armando Rigamonti − *Department of Materials Science INSTM Research Unit, University of Milano-Bicocca, 20125 Milan, Italy*

Charl X. Bezuidenhout − *Department of Materials Science INSTM Research Unit, University of Milano-Bicocca, 20125 Milan, Italy*

Jacopo Perego − *Department of Materials Science INSTM Research Unit, University of Milano-Bicocca, 20125 Milan, Italy*; orcid.org/0000-0003-4795-2060

Erica Montanari − *ENI Spa, R & D Dept., 20097 Milan, San Donato Milanese, Italy*

Complete contact information is available at: https://pubs.acs.org/10.1021/acs.chemmater.5c03237

Author Contributions

[§]A.R. and C.X.B. contributed equally to this work. J.P., S.B., C.B., and A.C. conceived the work. A.R., C.B., and J.P. developed synthetic strategies. J.P. and A.R. collected and elaborated the gas adsorption isotherms and breakthrough experiments. C.B. and A.R. elaborated the crystallographic data and theoretical calculations. S.B. elaborated MAS NMR spectra. ENI contributed to validating the data. S.B. and A.C. wrote the paper.

Funding

The work was supported by Eni S.p.A (DANTE project), the European Synchrotron Radiation Facility (ESRF, Grenoble, France) for the provision of beamtime at the ID22 beamline (proposal HC-5822), and the Ministero dell'Ambiente e della Sicurezza Energetica MASE (TESLA project: F57G25000060006).

Notes

The authors declare no competing financial interest.

■ ACKNOWLEDGMENTS

A.R. acknowledges the University of Messina for the Ph.D. program. The authors gratefully thank Meng He for technical assistance at the ESRF.

■ REFERENCES

(1) Abbass, K.; Qasim, M. Z.; Song, H.; Murshed, M.; Mahmood, H.; Younis, H. A review of the global climate change impacts, adaptation, and sustainable mitigation measures. *Environ. Sci. Pollut. Res.* **2022**, *29*, 42539−42559.

(2) Luis, P. Use of monoethanolamine (MEA) for CO_2 capture in a global scenario: Consequences and alternatives. *Desalination* **2016**, *380*, 93−99.

(3) Tan, J. Z. Y.; Uratani, J. M.; Griffiths, S.; Andresen, J. M.; Maroto-Valer, M. M. Chemistry advances driving industrial carbon capture technologies. *Nat. Rev. Chem.* **2025**, *9*, 656−671.

(4) Furukawa, H.; Cordova, K. E.; O'Keeffe, M.; Yaghi, O. M. The chemistry and applications of metal-organic frameworks. *Science* **2013**, *341* ((1−12)), No. 1230444.

(5) Sumida, K.; Rogow, D. L.; Mason, J. A.; McDonald, T. M.; Bloch, E. D.; Herm, Z. R.; Bae, T.-H.; Long, J. R. Carbon dioxide capture in metal−organic frameworks. *Chem. Rev.* **2012**, *112*, 724−781.

(6) Li, H.; Dilipkumar, A.; Abubakarb, S.; Zhao, D. Covalent organic frameworks for CO_2 capture: from laboratory curiosity to industry implementation. *Chem. Soc. Rev.* **2023**, *52*, 6294−6329.

(7) Song, K. S.; Fritz, P. W.; Coskun, A. Porous organic polymers for CO_2 capture, separation and conversion. *Chem. Soc. Rev.* **2022**, *51*, 9831−9852.

(8) Das, S.; Heasman, P.; Ben, T.; Qiu, S. Porous organic materials: strategic design and structure−function correlation. *Chem. Rev.* **2017**, *117*, 1515−1563.

(9) Perego, J.; Piva, S.; Bezuidenhout, C.; Comotti, A.; Sozzani, P.; Bracco, S. Direct Integration of Functionalized Bridges by One-step Superacid-Catalyzed Reaction to Fabricate Porous Polymers for CO_2 Capture and Separation. *Angew. Chem., Int. Ed.* **2025**, *64*, No. e202507863.

(10) Zou, L.; Sun, Y.; Che, S.; Yang, X.; Wang, X.; Bosch, M.; Wang, Q.; Li, H.; Smith, M.; Yuan, S.; Perry, Z.; Zhou, H.-C. Porous organic polymers for post-combustion carbon capture. *Adv. Mater.* **2017**, *29*, No. 1700229.

(11) Perego, J.; Piga, D.; Bracco, S.; Sozzani, P.; Comotti, A. Expandable porous organic frameworks with built-in amino and hydroxyl functions for CO_2 and CH_4 capture. *Chem. Commun.* **2018**, *54*, 9321−9324.

(12) Siegelman, R. L.; Kim, E. J.; Long, J. R. Porous materials for carbon dioxide separations. *Nat. Mater.* **2021**, *20*, 1060−1072.
(13) Lin, R.-B.; Chen, B. Hydrogen-bonded organic frameworks: Chemistry and functions. *Chem* **2022**, *8*, 2114−2135.
(14) Xing, G.; Bassanetti, I.; Bracco, S.; Negroni, M.; Bezuidenhout, C.; Ben, T.; Sozzani, P.; Comotti, A. A double helix of opposite charges to form channels with unique CO_2 selectivity and dynamics. *Chem. Sci.* **2019**, *10*, 730−736.
(15) Zhou, H.-C. J.; Kitagawa, S. Metal-organic frameworks (MOFs). *Chem. Soc. Rev.* **2014**, *43*, 5415−5418.
(16) Ding, M.; Flaig, R. W.; Long, J. H.; Yaghi, O. M. Carbon capture and conversion using metal−organic frameworks and MOF-based materials. *Chem. Soc. Rev.* **2019**, *48*, 2783−2828.
(17) Madden, D. G.; Scott, H. S.; Kumar, A.; Chen, K.-J.; Sanii, R.; Bajpai, A.; Lusi, M.; Curtin, T.; Perry, J. J.; Zaworotko, M. J. Flue-gas and direct-air capture of CO_2 by porous metal−organic materials. *Philos. Trans. R. Soc., A* **2017**, *375*, No. 20160025.
(18) Li, J. R.; Ma, Y.; McCarthy, M. C.; Sculley, J.; Yu, J.; Jeong, H. K.; Balbuena, P. B.; Zhou, H. -Cai Carbon dioxide capture-related gas adsorption and separation in metal-organic frameworks. *Coord. Chem. Rev.* **2011**, *255*, 1791−1823.
(19) Belmabkhout, Y.; Guillerm, V.; Eddaoudi, M. Low concentration CO_2 capture using physical adsorbents: are metal−organic frameworks becoming the new benchmark materials? *Chem. Eng. J.* **2016**, *296*, 386−397.
(20) Bose, S.; Sengupta, D.; Rayder, T. M.; Wang, X.; Kirlikovali, K. O.; Sekizkardes, A. K.; Islamoglu, T.; Farha, O. K. Challenges and opportunities: Metal−organic frameworks for direct air capture. *Adv. Funct. Mater.* **2024**, *34*, No. 2307478.
(21) Achenbach, B.; Yurdsen, A.; Stock, N.; Maurin, G.; Serre, C. Synthetic Aspects and Characterization Needs in MOF Chemistry—from Discovery to Applications. *Adv. Mater.* **2025**, *37*, No. 2411359.
(22) Lin, J.-B.; Nguyen, T. T. T.; Vaidhyanathan, R.; Burner, J.; Taylor, J. M.; Durekova, H.; Akhtar, F.; Mah, R. K.; Ghaffari-Nik, O.; Marx, S.; Fylstra, N.; Iremonger, S. S.; Dawson, K. W.; Sarkar, P.; Hovington, P.; Rajendran, A.; Woo, R. K.; Shimizu, G. A scalable metal-organic framework as a durable physisorbent for carbon dioxide capture. *Science* **2021**, *374*, 1464−1469.
(23) Nguyen, T. T. T.; Lin, J.-B.; Shimizu, G. K. H.; Rajendran, A. Separation of CO_2 and N_2 on a hydrophobic metal organic framework CALF-20. *Chem. Eng. J.* **2022**, *442* ((1−13)), No. 136263.
(24) Bette, S.; Sleptsova, A.; Lotsch, B. V.; Dinnebier, R. E.; Marx, S.; Loloei, M.; Adeleke, A. A.; Masoumifard, N.; Vaidhyanathan, R. CO_2 and H_2O Sorption Induced Bulk-Phase Changes of CALF-20 Captured Using In Situ Laboratory X-ray Powder Diffraction. *J. Am. Chem. Soc.* **2025**, *147*, 25662−25671.
(25) Kondo, M.; Okubo, T.; Asami, A.; Noro, S.-i.; Yoshitomi, T.; Kitagawa, S.; Ishii, T.; Matsuzaka, H.; Seki, K. Rational Synthesis of Stable Channel-Like Cavities with Methane Gas Adsorption Properties: [{Cu2(pzdc)2(L)}n] (pzdc = pyrazine-2,3-dicarboxylate; L = a Pillar Ligand). *Angew. Chem., Int. Ed.* **1999**, *38*, 140−143.
(26) ZareKarizi, F.; Joharian, M.; Morsali, A. Pillar-layered MOFs: functionality, interpenetration, flexibility and applications. *J. Mater. Chem. A* **2018**, *6*, 19288−19329.
(27) Senkovska, I.; Bon, V.; Abylgazina, L.; Mendt, M.; Berger, J.; Kieslich, G.; Petkov, P.; Fiorio, J. L.; Joswig, J.-O.; Heine, T.; Schaper, L.; Bachetzky, C.; Schmid, R.; Fischer, R. A.; Pöppl, A.; Brunner, E.; Kaskel, S. Understanding MOF flexibility: An analysis focused on pillared layer MOFs as a model system. *Angew. Chem., Int. Ed.* **2023**, *62*, No. e202218076.
(28) Hu, X.-L.; Liu, F.-H.; Wang, H.-N.; Qin, C.; Sun, C.-Y.; Su, Z.-M.; Liu, F.-C. Controllable synthesis of isoreticular pillared-layer MOFs: gas adsorption, iodine sorption and sensing small molecules. *J. Mater. Chem. A* **2014**, *2*, 14827−14834.
(29) Zhai, Q.-G.; Bai, N.; Li, S.; Bu, X.; Feng, P. Design of pore size and functionality in pillar-layered Zn-triazolate-dicarboxylate frameworks and their high CO_2/CH_4 and C2 hydrocarbons/CH_4 selectivity. *Inorg. Chem.* **2015**, *54*, 9862−9868.
(30) Gu, Y.-M.; Wang, Y.-H.; Zhao, S.-S.; Fan, H.-J.; Liu, X.-W.; Lai, Z.; Wang, S.-D. N-donating and water-resistant Zn-carboxylate frameworks for humid carbon dioxide capture from flue gas. *Fuel* **2023**, *336* ((1−8)), No. 126793.
(31) Yang, L.-Q.; Yu, J.; Zhang, P.; Wang, Y.; Yuan, W.-Y.; Zhai, Q.-G. Controllable C_2H_2/CO_2 inverse adsorption and separation in pillar-layered Zn-1,2,4-triazolate-dicarboxylate frameworks induced by the ligand aromaticity. *Sep. Purif. Technol.* **2023**, *327* ((1−10)), No. 124930.
(32) Klemenčič, K.; Krajnc, A.; Puškarić, A.; Huš, M.; Marinič, D.; Likozar, B.; Logar, N. Z.; Mazaj, M. Amine-Functionalized Triazolate-Based Metal−Organic Frameworks for Enhanced Diluted CO2 Capture Performance. *Angew. Chem., Int. Ed.* **2025**, *64*, No. e202424747.
(33) Julien, P. A.; Mottillo, C.; Friščić, T. Metal−organic frameworks meet scalable and sustainable synthesis. *Green Chem.* **2017**, *19*, 2729−2747.
(34) Stolar, T.; Užarević, K. Mechanochemistry: an efficient and versatile toolbox for synthesis, transformation, and functionalization of porous metal−organic frameworks. *CrystEngComm* **2020**, *22*, 4511−4525.
(35) Gao, T.; Tang, H. J.; Zhang, S. Y.; Cao, J. W.; Wu, Y. N.; Chen, J.; Wang, Y.; Chen, K. J. Mechanochemical synthesis of three-component metal-organic frameworks for large scale production. *J. Solid State Chem.* **2021**, *303*, No. 122547.
(36) Marrett, J. M.; Effaty, F.; Ottenwaelder, X.; Friščić, T. Mechanochemistry for metal−organic frameworks and covalent−organic frameworks (MOFs, COFs): methods, materials, and mechanisms. *Adv. Mater.* **2025**, *37*, No. 2418707.
(37) Guillerm, V.; Kim, D.; Eubank, J. F.; Luebke, R.; Liu, X.; Adil, K.; Lah, M. S.; Eddaoudi, M. A supermolecular building approach for the design and construction of metal−organic frameworks. *Chem. Soc. Rev.* **2014**, *43*, 6141−6172.
(38) Singh, P.; Singh, H. D.; Menonab, A. H.; Vaidhyanathan, R. Preferential CO_2 adsorption by an ultra-microporous zinc-amino-triazolato-acetate MOF. *Chem. Commun.* **2023**, *59*, 5559−5562.
(39) Xiao, C.; Tian, J.; Chen, Q.; Hong, M. Water-stable metal−organic frameworks (MOFs): rational construction and carbon dioxide capture. *Chem. Sci.* **2024**, *15*, 1570−1610.
(40) Xiong, S.; Gong, Y.; Wang, H.; Wang, H.; Liu, Q.; Gu, M.; Wang, X.; Chen, B.; Wang, Z. A new tetrazolate zeolite-like framework for highly selective CO_2/CH_4 and CO_2/N_2 separation. *Chem. Commun.* **2014**, *50*, 12101−12104.
(41) Thommes, M.; Kaneko, K.; Neimark, A. V.; Olivier, J. P.; Rodriguez-Reinoso, F.; Rouquerol, J.; Sing, K. S. W. Physisorption of gases, with special reference to the evaluation of surface area and pore size distribution. *Pure Appl. Chem.* **2015**, *87*, 1051−1069.
(42) Rajendran, A.; Shimizu, G. K. H.; Woo, T. K. The Challenge of Water Competition in Physical Adsorption of CO_2 by Porous Solids for Carbon Capture Applications − A Short Perspective. *Adv. Mater.* **2024**, *36*, No. 2301730.

https://doi.org/10.1021/acs.chemmater.5c03237
Chem. Mater. 2026, 38, 4038−4045